LETTERS

Measuring mechanical tension across vinculin reveals regulation of focal adhesion dynamics

Carsten Grashoff[1,2]*, Brenton D. Hoffman[1,2]*, Michael D. Brenner[3,4], Ruobo Zhou[3], Maddy Parsons[5], Michael T. Yang[6], Mark A. McLean[7], Stephen G. Sligar[7], Christopher S. Chen[6], Taekjip Ha[3,4,8] & Martin A. Schwartz[1,2,9]

Mechanical forces are central to developmental, physiological and pathological processes[1]. However, limited understanding of force transmission within sub-cellular structures is a major obstacle to unravelling molecular mechanisms. Here we describe the development of a calibrated biosensor that measures forces across specific proteins in cells with piconewton (pN) sensitivity, as demonstrated by single molecule fluorescence force spectroscopy[2]. The method is applied to vinculin, a protein that connects integrins to actin filaments and whose recruitment to focal adhesions (FAs) is force-dependent[3]. We show that tension across vinculin in stable FAs is ~2.5 pN and that vinculin recruitment to FAs and force transmission across vinculin are regulated separately. Highest tension across vinculin is associated with adhesion assembly and enlargement. Conversely, vinculin is under low force in disassembling or sliding FAs at the trailing edge of migrating cells. Furthermore, vinculin is required for stabilizing adhesions under force. Together, these data reveal that FA stabilization under force requires both vinculin recruitment and force transmission, and that, surprisingly, these processes can be controlled independently.

Focal adhesions (FAs) are complex intracellular linkages between integrins and the F-actin cytoskeleton that both transmit and respond to mechanical forces. FAs show complex mechanosensitivity such that they form or enlarge when force increases, and shrink or disassemble when force decreases[3]. However, mechanical forces can also induce FA disassembly, including sliding, a form of controlled disassembly[4]. In the absence of a method to measure forces across proteins in cells, these distinct processes have been difficult to elucidate and are poorly understood.

Vinculin is an intracellular FA protein comprised of a head domain (Vh) and a tail domain (Vt) separated by a flexible linker[5]. Binding of Vh to talin recruits vinculin to FAs, whereas Vt binds to F-actin and paxillin[6]. Interestingly, vinculin seems intimately linked to FA mechanosensitivity. Its recruitment to FAs is regulated by externally or internally generated mechanical forces[7,8]; vinculin-deficient cells display impaired cell spreading and cell migration, are less stiff than normal cells and exert lower traction forces[9–11]. Furthermore, vinculin seems to be a key element in the molecular 'clutch' that links the actin cytoskeleton and extracellular matrix[12], and colocalizes with areas of high force during leading edge protrusion[13]. These and other data have led to the concept of adhesion strengthening, in which adhesions under force recruit additional vinculin and enlarge to keep force per area constant[14,15]. However, where and when forces across vinculin occur on the sub-cellular level is unknown. Indeed, direct evidence that vinculin bears mechanical force is absent. Estimates from traction force microscopy suggest that tension across molecules in FAs is in the piconewton range[14,16], a factor of 10–50 below the resolution of existing methods to measure forces across proteins within cells[17]. We therefore developed a genetically encoded vinculin tension sensor with single piconewton sensitivity for use in living cells.

We designed a tension sensor module (TSMod) in which a 40-amino-acid-long elastic domain was inserted between two fluorophores (mTFP1 and venus(A206K)) that undergo efficient fluorescence resonance energy transfer (FRET) (Fig. 1a)[18]. The elastic domain was derived from the spider silk protein flagelliform, which

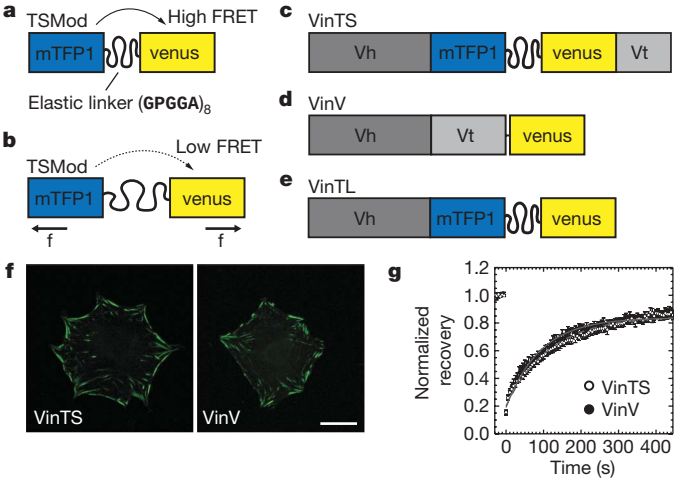

Figure 1 | Vinculin tension sensor (VinTS) constructs. a, The tension sensor module (TSMod) consists of two fluorophores separated by a flagelliform linker sequence $(GPGGA)_8$. **b**, When force across TSMod extends the elastic linker, FRET efficiency decreases (f, force). **c**, The vinculin tension sensor (VinTS) consists of TSMod inserted after amino acid 883 of vinculin. **d**, Vinculin–venus control (VinV). **e**, Vinculin tail-less control (VinTL). **f**, Localization of VinTS and VinV in vinculin$^{-/-}$ cells. Scale bar, 20 μm. **g**, Normalized average fluorescence recovery rates of VinTS (open circles, $n = 10$) and VinV (closed circles, $n = 8$). Error bars represent standard error of the mean (s.e.m.). (Recovery half-time VinTS: 87.6 ± 6.6 s, VinV: 68.3 ± 13.1 s; mean ± s.e.m., $P = 0.205$).

[1]Robert M. Berne Cardiovascular Research Center, University of Virginia, Charlottesville, Virginia 22908, USA. [2]Department of Microbiology, University of Virginia, Charlottesville, Virginia 22908, USA. [3]Center for the Physics of Living Cells and Department of Physics, University of Illinois at Urbana-Champaign, Urbana, Illinois 61801, USA. [4]Department of Chemistry, University of Illinois at Urbana-Champaign, Urbana, Illinois 61801, USA. [5]Randall Division of Cell and Molecular Biophysics, King's College London, London SE1 1UL, UK. [6]Department of Bioengineering, University of Pennsylvania, Philadelphia, Pennsylvania, 19104, USA. [7]Department of Biochemistry, University of Illinois at Urbana-Champaign, Urbana, Illinois 61801, USA. [8]Howard Hughes Medical Institute, Urbana, Illinois 61801, USA. [9]Department of Biomedical Engineering, University of Virginia, Charlottesville, Virginia 22908, USA.
*These authors contributed equally to this work.

is composed of repetitive amino-acid motifs that form entropic nanosprings suitable for measuring piconewton forces[19]. Since FRET is highly sensitive to the distance between the fluorophores, FRET efficiency should decrease under tension (Fig. 1b). The vinculin tension sensor contains the sensor module between the Vh and Vt domain of vinculin after amino acid 883 (VinTS, Fig. 1c). Controls include a carboxy-terminally tagged vinculin–venus (VinV, Fig. 1d) and a tail-less mutant, which cannot bind F-actin or paxillin (VinTL, Fig. 1e). Thus, tension cannot be applied to the VinTL construct.

In transiently transfected vinculin$^{-/-}$ cells, VinTS was properly recruited to FAs. FA shape and size, and F-actin organization were indistinguishable from cells expressing VinV (Fig. 1f and Supplementary Fig. 1a, b, e). Cells expressing VinTL had significantly enlarged FAs, consistent with previous studies[20] (Supplementary Fig. 1c, e). TSMod localized to the cytoplasm and the nucleus (Supplementary Fig. 1d). All constructs produced stable proteins with the expected molecular size (Supplementary Fig. 2a). Expression of VinTS in vinculin$^{-/-}$ cells was comparable to the level of endogenous vinculin in murine embryonic fibroblasts (MEFs) or bovine aortic endothelial cells (BAECs) (Supplementary Fig. 2b).

Next, we probed the activation state of VinTS. In solution, binding of Vh to Vt induces a closed, auto-inhibited conformation that does not bind F-actin. However, F-actin and the bacterial protein IpaA bind cooperatively to vinculin to induce its activation[21]. High-speed centrifugation of hypotonic cell lysates from cells expressing VinTS or VinV to sediment F-actin co-sedimented only a small amount of either vinculin construct, even when actin was supplemented. Addition of IpaA alone modestly increased sedimentation, presumably due to vinculin binding to endogenous actin in cell lysates. IpaA and actin together induced nearly complete sedimentation of both vinculin constructs (Supplementary Fig. 2c). Furthermore, fluorescence recovery after photobleaching (FRAP) in live cells showed that recovery rates in FAs were similar between VinTS and VinV, indicating normal vinculin dynamics[22] (Fig. 1g). Thus, insertion of TSMod does not significantly affect vinculin's localization to FAs, its activation state, actin binding, or intracellular dynamics.

We next tested for two potential confounding factors, intermolecular FRET and effects of vinculin conformation on FRET (FRET metrics are explained in Supplementary Note 2). When cells were transfected with both vinculin–mTFP1 and vinculin–venus(A206K) (fluorophore insertion after amino acid 883), the FRET index in FAs was very low compared to cells expressing VinTS, indicating that intermolecular FRET is negligible (Supplementary Fig. 3a–c). To examine effects of conformational changes during vinculin activation, we used IpaA and actin to activate vinculin. As a positive control, we generated a mTFP1–venus(A206K) version of a previously described vinculin conformation FRET probe[21] (VinCS, Supplementary Fig. 3d). Spectrofluorometric analysis of hypotonic cell lysates containing these constructs showed that, as expected, adding neither actin nor IpaA alone affected FRET efficiency of VinCS, whereas IpaA plus actin decreased FRET efficiency. In contrast, VinTS showed no change in FRET efficiency under identical conditions (Supplementary Fig. 3e). Thus, vinculin's conformational changes do not affect FRET efficiency of VinTS.

To evaluate responses to cellular forces, vinculin$^{-/-}$ cells expressing VinTS or VinTL were seeded on fibronectin- or poly-L-lysine-coated coverslips. Cells on fibronectin rapidly spread and formed FAs, whereas cells on poly-L-lysine remained round, with the constructs diffusely distributed in the cytoplasm. FRET was high for both constructs on poly-L-lysine (Fig. 2a). Spectrofluorometry of hypotonic cell lysates, another zero-force state, also showed no difference between VinTS, VinTL and TSMod in solution (Fig. 2b). In contrast, VinTS, but not VinTL, displayed reduced FRET index in FAs on fibronectin, indicating increased mechanical tension (Fig. 2a). These results were confirmed by fluorescence lifetime microscopy (FLIM)[23]. In adherent cells, VinTS had significantly longer lifetimes (corresponding to lower FRET efficiency, see Supplementary Note 2). Lifetimes were

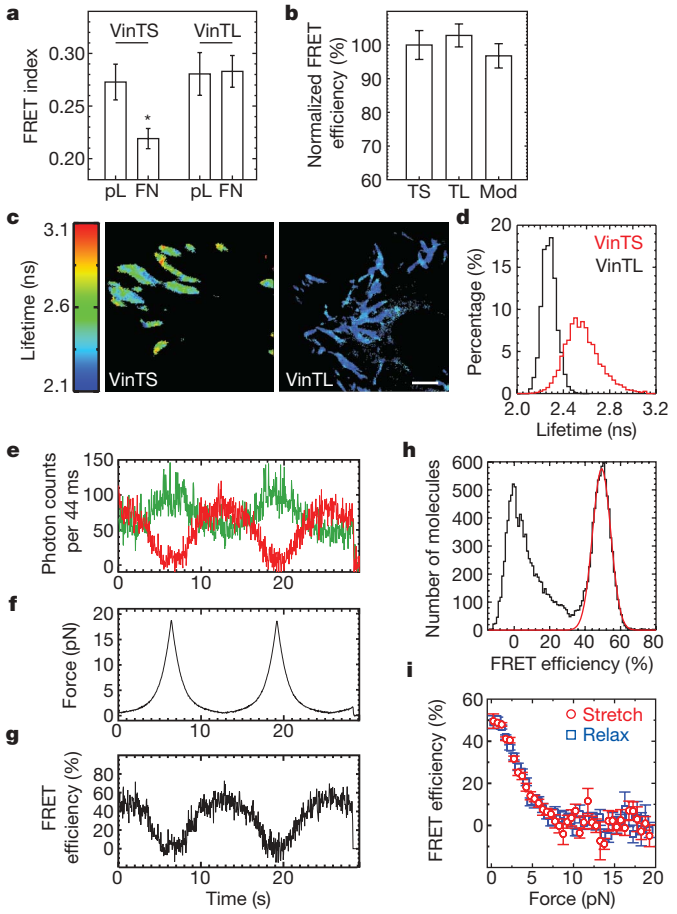

Figure 2 | Responses to mechanical force. **a**, FRET index in vinculin$^{-/-}$ cells expressing VinTS or VinTL seeded on poly-L-lysine (pL) or fibronectin (FN) (*$P < 0.05$, Tukey-b test, $n = 11$–18). **b**, FRET measured by spectrofluorometry of lysates containing VinTS, VinTL or TSMod ($n = 4$, $P > 0.5$, Tukey-b test). **c**, Fluorescence lifetime images of vinculin$^{-/-}$ cells expressing VinTS or VinTL. Scale bar, 2 μm. **d**, Fluorescence lifetime histograms from FAs of VinTS ($n = 11$) or VinTL ($n = 8$) expressing vinculin$^{-/-}$ cells. **e–g**, Multiple stretch/relax cycles of a single TSModCy using fluorescence force spectroscopy. **e**, Fluorescence intensity time traces for donor (green) and acceptor (red). **f**, Applied force versus time. **g**, FRET efficiency versus time. **h**, Single-molecule FRET histogram of TSModCy at zero force. The peak marked by a red Gaussian fit represents the TSModCy labelled with both donor and acceptor. **i**, Averaged FRET–force curves from $n = 7$ molecules show reversible stretching and relaxing of TSModCy between 0.25 and 19 pN. All error bars represent s.e.m.

also distributed over a much wider range than VinTL, indicating that individual molecules are subject to a range of forces (Fig. 2c, d).

To calibrate the tension sensor, we used single-molecule fluorescence force spectroscopy, which combines confocal scanning fluorescence microscopy with optical tweezers[2]. Because fluorescent proteins' low photostability precludes single-molecule FRET measurements, we generated a version of TSMod using the organic fluorophores Cy3 and Cy5 (TSModCy, Supplementary Fig. 4a). The flagelliform linker (F40) was connected to a polymer-coated glass surface via 18 base pair long double-stranded (ds) DNA and to a microsphere held in tweezers through ~50 kilobase dsDNA. DNA tethers presented the fluorophores in close proximity to terminal cysteine residues of F40, allowing estimation of the linker end-to-end distance as a function of force from FRET measurements (Supplementary Fig. 4a). Changes in FRET efficiency over multiple force cycles showed that TSModCy reached conformational equilibrium rapidly and displayed no hysteresis, indicating reversibility (Fig. 2e–g). The zero-force FRET efficiency of ~50% determined separately (Fig. 2h) matched the FRET value at the lowest force

analysed (0.25 pN, Fig. 2i), indicating no adverse effects due to linkers or the optical tweezer. Together, these experiments showed that TSModCy is most sensitive at 1–6 pN (Fig. 2i).

These measurements were used to estimate the force sensitivity of TSMod (Supplementary Fig. 4b and Supplementary Note 3) and to calculate forces across vinculin in living cells using FLIM microscopy data. This analysis showed that the average force in stationary FAs is ~2.5 pN (Supplementary Fig. 4c–e). The assumptions underlying this analysis and the inherent limitations are discussed in Supplementary Note 3.

Vinculin recruitment to FAs is force-dependent[7,8]. To test whether recruitment correlates with force transmission across vinculin, we treated cells with a Rho-associated kinase (ROCK) inhibitor (Y-27632) to reduce myosin-dependent contractility. Alternatively, we depleted myosin IIa (MIIa) by RNA interference (Supplementary Fig. 5). Both treatments reduced FA size and traction forces were moderately reduced, as expected[24] (data not shown and Fig. 3a), but vinculin was still localized in FAs (Supplementary Fig. 5c and data not shown). Interestingly, the FRET index of VinTS increased to the level of VinTL, indicating a drastic loss of tension across vinculin (Fig. 3b). By contrast, the vinculin conformation sensor (Supplementary Fig. 3d) showed only a slight increase in FRET index after treating cells with Y-27632, indicating that most of vinculin remained in an open conformation (Fig. 3c). These data demonstrate that vinculin activation and recruitment to FAs are separable from transmission of force across vinculin.

We next examined mechanical forces across vinculin during cell migration. To ensure sufficient statistical power for the subcellular analysis, individual FAs were isolated and averaged (Supplementary Fig. 6 and Supplementary Note 2). In BAECs, vinculin within small FAs near protruding edges and occasionally in the centre of moving cells showed low FRET index indicating high tension, whereas large retracting FAs showed high FRET index indicating lower force per

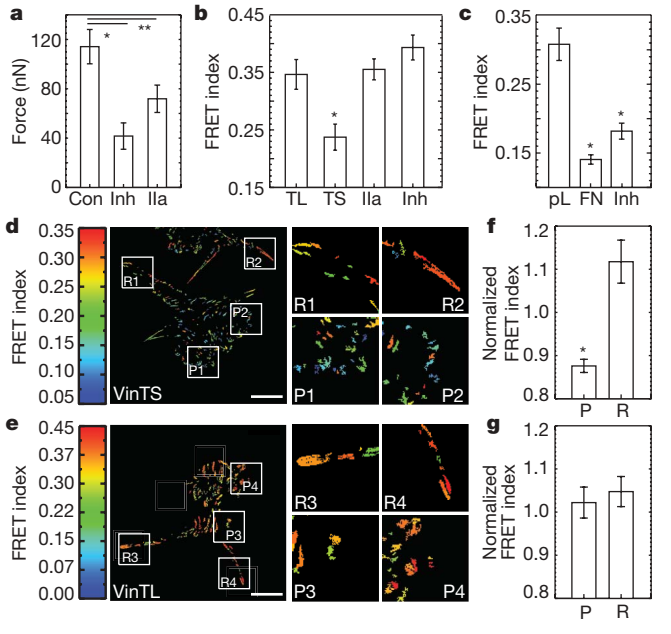

Figure 3 | Forces across vinculin during cell migration. **a**, Traction forces of VinTS-expressing cells (Con, $n = 18$), treated with Y-27632 (Inh, $n = 15$) or depleted of myosin IIa (IIa, $n = 20$) ($^*P < 0.005$, $^{**}P < 0.05$, Dunnett's test). **b**, FRET index of VinTL and VinTS, or VinTS after IIa and Inh ($n = 30$, $^*P < 0.005$, Tukey-b test). **c**, Cells expressing VinCS on poly-L-lysine, fibronectin, or fibronectin after treatment with Y-27632 (Inh) ($n = 30$, $^*P < 5 \times 10^{-6}$, Tukey-b test). **d**, FRET index of VinTS in BAECs. P, protruding areas; R, retracting areas. **e**, FRET index of VinTL in BAECs. Scale bars, 20 μm. **f**, **g**, FRET index of protruding (P) and retracting (R) areas normalized by FRET index of all FAs. **f**, VinTS ($n = 4$, $^*P < 0.01$). **g**, VinTL ($n = 4$, $P > 0.5$). All error bars represent s.e.m.

vinculin (Fig. 3d, f and Supplementary Movie 1). The VinTL control displayed uniformly high FRET index at all locations (Fig. 3e, g and Supplementary Movie 2; data normalization explained in Supplementary Note 2).

To examine this in more detail, we generated custom software to isolate and track FAs and correlate their dynamics with FRET (Supplementary Note 2). Analysis of spreading or migrating vinculin$^{-/-}$ cells expressing VinTS revealed that force on vinculin was very high in small FAs that first appeared at cell edges, but decreased towards average levels as they enlarged (Fig. 4a and Supplementary Fig. 7). Conversely, as FAs disassembled, forces across vinculin remained low and even slightly decreased (Fig. 4b and Supplementary Fig. 7). These effects were not observed with VinTL (Supplementary Fig. 8). Previous studies showed that FA sliding or disassembly at retracting edges is associated with high local Rho-[25] and myosin-activation and is myosin-dependent[26], suggesting that the adhesions in retracting regions are under force. The low force on vinculin is therefore surprising but consistent with predictions based on intracellular force reconstructions from actin speckle analyses[13]. These data confirm that vinculin recruitment and force bearing are separable, and they indicate that failure of vinculin to bear force is linked to disassembly.

We therefore tested whether vinculin is required for FA stabilization under force. Under normal culture conditions, vinculin$^{-/-}$ cells or cells expressing vinculin–Flag displayed similar FA dynamics, visualized by enhanced green fluorescent protein (EGFP)–paxillin (Fig. 4c and Supplementary Fig. 9a). However, co-expressing either myosin IIa or active RhoA stabilized FAs in cells that contained vinculin, but not in vinculin-deficient cells (Fig. 4d, e and Supplementary Fig. 9b, c). In vinculin$^{-/-}$ cells, increased contractility often led to entire sides of the cell retracting, followed by formation of new protrusions. Indeed, FA behaviour at the periphery of vinculin$^{-/-}$ cells strongly resembled the trailing edge of migrating cells where force across vinculin was low (Supplementary Fig. 9 and Supplementary Movies 3–8). Thus, vinculin is required for FA stabilization under tension.

Taken together, these data reveal an unexpected regulatory mechanism in which the ability of vinculin to bear force determines whether

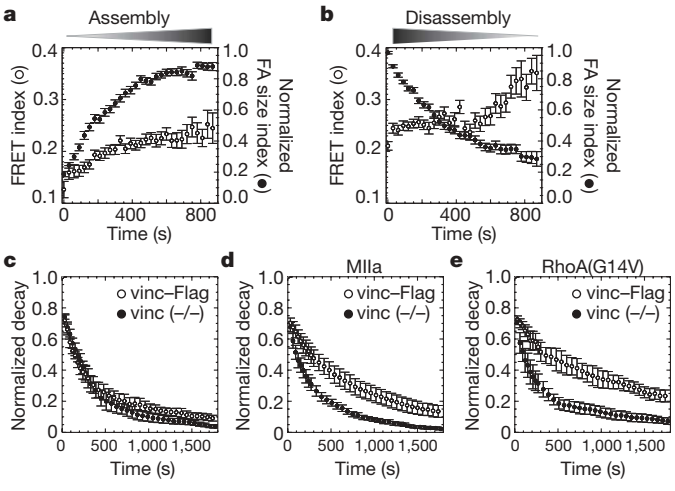

Figure 4 | Tension on vinculin in dynamic FAs. FAs were isolated, tracked and classified as assembling or disassembling. **a**, In assembling FAs ($n = 78$), FRET index (open circles) increased with normalized FA size index (defined in Supplementary Note 2, closed circles). **b**, In disassembling FAs ($n = 92$), FRET index was high and further increased at late stages. **c**, Lifetime of FAs visualized with EGFP–paxillin in vinculin$^{-/-}$ cells (vinc (−/−); $n = 4$ cells, 214 FAs) or cells re-expressing vinculin–Flag (vinc–Flag; $n = 4$ cells, 310 FAs). Difference at 870 s was not significant ($P = 0.24$). **d**, FA lifetime in vinculin$^{-/-}$ cells ($n = 7$ cells, 408 FAs) and vinculin–Flag cells ($n = 7$ cells, 715 FAs) expressing MIIa (difference at 870 s: $P < 0.005$). **e**, Vinculin$^{-/-}$ cells ($n = 3$ cells, 250 FAs) or vinculin–Flag cells ($n = 3$ cells, 192 FAs) expressing active RhoA(G14V) (difference at 870 s: $P < 0.05$). All error bars represent s.e.m.

adhesions assemble or disassemble under tension. Although creating new biosensors is always challenging (Supplementary Note 3), this genetically encoded tension sensor with piconewton sensitivity should be applicable to other molecules involved in force transmission and mechanotransduction.

METHODS SUMMARY

Generation and characterization of expression constructs. For detailed information on the generation of cDNA constructs see Supplementary Note 1. Immunostaining and western blotting were performed using standard protocols. Expression and purification of glutathione *S*-transferase (GST)–IpaA, and the vinculin-sedimentation assay were described elsewhere[21].

FRET analysis. Calculations were performed with custom-written programs in IDL (ITT Visual Information Systems). The pFRET algorithm was implemented for nonlinear bleed-through corrections[27]. FRET index is the corrected FRET divided by acceptor intensity. FAs were identified in the venus(A206K) channel using the water algorithm[28], and used as masks for local averaging. For more detailed information see Supplementary Note 2.

FRAP and FA dynamics analysis. For FRAP analysis, bleached and control FAs were identified by the water algorithm and polygons were automatically moved for slow-moving FAs. Recovery curves were analysed as described[22]. FA dynamics were analysed in vinculin$^{-/-}$ cells expressing EGFP–paxillin. FA decay curves were generated as described[29] except that individual FA curves were generated, normalized and averaged. Particle tracking was performed as described previously[30] with particle centres determined by the water algorithm. Trajectory accuracy and selection of dynamic FAs were determined manually (Supplementary Note 2).

FLIM analysis. Time-domain FLIM experiments and FLIM data analysis were performed as described previously[23] using TRI2 software (developed by P. Barber, Gray Cancer Institute, UK). Fluorescence lifetime was determined by fitting a single-exponential decay model, as mTFP1 modification was uniform within a pixel. With 890 nm excitation, acquisition times up to 150 s achieved sufficient photon statistics.

***In vitro* force calibration.** The 40 amino acid long flagelliform peptide $(GPGGA)_8$ was crosslinked to maleimide-functionalized DNA. The peptide–DNA conjugate was labelled with organic fluorophores for fluorescence-force spectroscopy to determine the force per end-to-end distance of the peptide. For more detailed information see Online Methods and Supplementary Note 3.

Full Methods and any associated references are available in the online version of the paper at www.nature.com/nature.

Received 8 February; accepted 25 May 2010.

1. Orr, A. W., Helmke, B. P., Blackman, B. R. & Schwartz, M. A. Mechanisms of mechanotransduction. *Dev. Cell* **10,** 11–20 (2006).
2. Hohng, S. *et al.* Fluorescence-force spectroscopy maps two-dimensional reaction landscape of the Holliday junction. *Science* **318,** 279–283 (2007).
3. Bershadsky, A. D., Balaban, N. Q. & Geiger, B. Adhesion-dependent cell mechanosensitivity. *Annu. Rev. Cell Dev. Biol.* **19,** 677–695 (2003).
4. Ballestrem, C., Hinz, B., Imhof, B. A. & Wehrle-Haller, B. Marching at the front and dragging behind: differential αVβ3-integrin turnover regulates focal adhesion behavior. *J. Cell Biol.* **155,** 1319–1332 (2001).
5. Bakolitsa, C. *et al.* Structural basis for vinculin activation at sites of cell adhesion. *Nature* **430,** 583–586 (2004).
6. Ziegler, W. H., Gingras, A. R., Critchley, D. R. & Emsley, J. Integrin connections to the cytoskeleton through talin and vinculin. *Biochem. Soc. Trans.* **36,** 235–239 (2008).
7. Galbraith, C. G., Yamada, K. M. & Sheetz, M. P. The relationship between force and focal complex development. *J. Cell Biol.* **159,** 695–705 (2002).
8. Riveline, D. *et al.* Focal contacts as mechanosensors: externally applied local mechanical force induces growth of focal contacts by an Mdia1-dependent and ROCK-independent mechanism. *J. Cell Biol.* **153,** 1175–1186 (2001).
9. Xu, W., Baribault, H. & Adamson, E. D. Vinculin knockout results in heart and brain defects during embryonic development. *Development* **125,** 327–337 (1998).
10. Alenghat, F. J. *et al.* Analysis of cell mechanics in single vinculin-deficient cells using a magnetic tweezer. *Biochem. Biophys. Res. Commun.* **277,** 93–99 (2000).
11. Mierke, C. T. *et al.* Mechano-coupling and regulation of contractility by the vinculin tail domain. *Biophys. J.* **94,** 661–670 (2008).
12. Hu, K. *et al.* Differential transmission of actin motion within focal adhesions. *Science* **315,** 111–115 (2007).
13. Ji, L., Lim, J. & Danuser, G. Fluctuations of intracellular forces during cell protrusion. *Nature Cell Biol.* **10,** 1393–1400 (2008).
14. Balaban, N. Q. *et al.* Force and focal adhesion assembly: a close relationship studied using elastic micropatterned substrates. *Nature Cell Biol.* **3,** 466–472 (2001).
15. Shemesh, T., Geiger, B., Bershadsky, A. D. & Kozlov, M. M. Focal adhesions as mechanosensors: a physical mechanism. *Proc. Natl Acad. Sci. USA* **102,** 12383–12388 (2005).
16. Tan, J. L. *et al.* Cells lying on a bed of microneedles: an approach to isolate mechanical force. *Proc. Natl Acad. Sci. USA* **100,** 1484–1489 (2003).
17. Meng, F., Suchyna, T. M. & Sachs, F. A fluorescence energy transfer-based mechanical stress sensor for specific proteins in situ. *FEBS J.* **275,** 3072–3087 (2008).
18. Day, R. N., Booker, C. F. & Periasamy, A. Characterization of an improved donor fluorescent protein for Forster resonance energy transfer microscopy. *J. Biomed. Opt.* **13,** 031203 (2008).
19. Becker, N. *et al.* Molecular nanosprings in spider capture-silk threads. *Nature Mater.* **2,** 278–283 (2003).
20. Humphries, J. D. *et al.* Vinculin controls focal adhesion formation by direct interactions with talin and actin. *J. Cell Biol.* **179,** 1043–1057 (2007).
21. Chen, H. *et al.* Spatial distribution and functional significance of activated vinculin in living cells. *J. Cell Biol.* **169,** 459–470 (2005).
22. Cohen, D. M. *et al.* A conformational switch in vinculin drives formation and dynamics of a talin-vinculin complex at focal adhesions. *J. Biol. Chem.* **281,** 16006–16015 (2006).
23. Parsons, M. *et al.* Quantification of integrin receptor agonism by fluorescence lifetime imaging. *J. Cell Sci.* **121,** 265–271 (2008).
24. Cai, Y. *et al.* Nonmuscle myosin IIA-dependent force inhibits cell spreading and drives F-actin flow. *Biophys. J.* **91,** 3907–3920 (2006).
25. Pertz, O., Hodgson, L., Klemke, R. L. & Hahn, K. M. Spatiotemporal dynamics of RhoA activity in migrating cells. *Nature* **440,** 1069–1072 (2006).
26. Kolega, J. Asymmetric distribution of myosin IIB in migrating endothelial cells is regulated by a rho-dependent kinase and contributes to tail retraction. *Mol. Biol. Cell* **14,** 4745–4757 (2003).
27. Periasamy, A., Wallrabe, H., Chen, Y. & Barroso, M. Chapter 22: Quantitation of protein-protein interactions: confocal FRET microscopy. *Methods Cell Biol.* **89,** 569–598 (2008).
28. Zamir, E. *et al.* Molecular diversity of cell-matrix adhesions. *J. Cell Sci.* **112,** 1655–1669 (1999).
29. Zaidel-Bar, R., Milo, R., Kam, Z. & Geiger, B. A paxillin tyrosine phosphorylation switch regulates the assembly and form of cell-matrix adhesions. *J. Cell Sci.* **120,** 137–148 (2007).
30. Crocker, J. C. & Hoffman, B. D. Multiple-particle tracking and two-point microrheology in cells. *Methods Cell Biol.* **83,** 141–178 (2007).

Supplementary Information is linked to the online version of the paper at www.nature.com/nature.

Acknowledgements We thank R. Horwitz, M. Vicente-Manzanares, D. Schafer, L. K. Tamm and K. A. DeMali for reagents and M. Gardel for critical reading of the manuscript. This work was supported by USPHS grant U54 GM64346 to M.A.S., C.G. was supported by a Research Fellowship from the Deutsche Forschungsgemeinschaft (DFG, GR3399/1-1). B.D.H. was supported by USPHS training grant 5T32-HL007284 and an AHA Postdoctoral Fellowship. M.D.B., R.Z. and T.H. were supported by the US National Science Foundation Physics Frontier Center grant 0822613 and by USPHS grant R21 RR025341. T.H. is an investigator with the Howard Hughes Medical Institute. M.P. was supported by a Royal Society University Research Fellowship (UK). M.T.Y. was supported by an IGERT fellowship from the National Science Foundation (DGE-0221664).

Author Contributions M.A.S. conceived the general idea. C.G. conceived the use of the flagelliform sequence, designed and generated vinculin expression constructs, performed spectrofluorometry and all cell and imaging experiments. B.D.H. generated analysis tools and analysed the *in vivo* data. T.H., M.A.M. and S.G.S. conceived the sensor calibration scheme. M.D.B. designed and generated the tension sensor construct for the calibration. M.D.B. and R.Z. performed and analysed the single molecule experiments. T.H., R.Z., M.D.B and B.D.H. developed an algorithm to map *in vitro* and *in vivo* tension sensor data. M.P. performed and analysed FLIM experiments. M.T.Y and C.S.C. generated micropost arrays and analysed traction force data. C.G., B.D.H. and M.A.S. designed the *in vivo* experiments, discussed the results and wrote the paper with input from all authors.

Author Information Reprints and permissions information is available at www.nature.com/reprints. The authors declare no competing financial interests. Readers are welcome to comment on the online version of this article at www.nature.com/nature. Correspondence and requests for materials should be addressed to M.A.S. (maschwartz@virginia.edu), except those on single-molecule force calibration, which should be addressed to T.H. (tjha@illinois.edu).

METHODS

Statistics. Statistical significance was determined by Student's *t*-test, one-way or two-way analysis of variance (ANOVA), as appropriate. Post-hoc testing was done with Dunnet's or Tukey-b test as indicated. Calculations were performed with SPSS (SPSS Inc.) or Excel (Microsoft).

Antibodies. Antibodies used in this study include: monoclonal anti-paxillin (BD Transduction), AlexaFluor 647 goat-anti-mouse, monoclonal anti-tubulin E7 (Developmental Studies Hybridoma Bank), monoclonal anti-vinculin (Sigma), monoclonal anti-GFP (Santa Cruz), anti-non-muscle myosin heavy chain IIa (Covance), anti-mouse–horseradish peroxidase (HRP) and anti-rabbit–HRP (Jackson ImmunoResearch). Phalloidin–AlexaFluor 568 was from Molecular Probes.

Cell culture conditions and live cell microscopy. Vinculin$^{-/-}$ cells, BAECs, MEFs and HEK293 cells were cultured in DMEM containing non-essential amino acids, penicillin/streptomycin (Gibco) and 10% calf serum (Atlanta Biologicals). Live cell experiments used phenol-red free DMEM (Gibco). Cells were seeded on No. 1.5 microscope cover glasses (Corning) coated with 2.5 μg ml^{-1} fibronectin (for BAECs), 10 μg ml^{-1} fibronectin or 20 μg ml^{-1} poly-L-lysine (for vinculin$^{-/-}$ cells). To inhibit contractility, cells were treated with 10 μM Y-27632 (Sigma) for 2 h. Images for FRET, FRAP and FA stability analysis were obtained using a Zeiss LSM510 confocal microscope with a Plan-Neofluor ×40 NA = 1.3 DIC objective or a Plan-Apochromat ×100 NA = 1.4 objective and an argon laser featuring 458 and 514 nm laser lines. For FRET experiments a HFT 458/514 beam splitter and the following filters were used: mTFP1, band-pass 470–500; venus/FRET, band-pass 530–600.

Traction force imaging and analysis. Polydimethylsiloxane (PDMS)-based micropost arrays (mPADs) were used to report cellular traction forces as described previously[16]. To measure traction forces, fluorescent images of the microposts were acquired at focal planes passing through the tip and base of the microposts. Images were taken with a Nikon TE 300 equipped with a violet-corrected Plan Apo ×60 NA = 1.4 DIC objective and 655 long pass filter set. A custom-written program (Matlab) was used to extract the centroids of the microposts at the tip and base, representing the deflected and undeflected positions. Micropost deflections were converted into forces by multiplying with a spring constant of 7.22 nN μm^{-1}.

FLIM experiments and analysis. Time-domain FLIM was performed with a multi-photon microscope system as described previously[23]. The system is based on a modified Bio-Rad MRC 1024MP workstation, comprising a solid-state-pumped femto-second Ti:Sapphire laser system (Tsunami, Spectra-Physics), a focal scan-head and an inverted microscope (Nikon TE2000), and a ×40 Nikon CFI Plan Fluor NA = 1.3 objective. Enhanced detection of the scattered component of the emitted photons was afforded by the use of fast response (Hamamatsu R7401-P) non-descanned detectors, developed in-house, situated in the re-imaged objective pupil plane. Fluorescence lifetime imaging capability was provided by time-correlated single photon counting (TCSPC) electronics (Becker & Hickl, SPC 700). Data were collected at 500 ± 20 nm through a band-pass filter (Coherent Inc. 35-5040). Laser power was adjusted to give average photon counting rates of the order 10^4–10^5 photons s^{-1} (0.0001 to 0.001 photon counts per excitation event) to avoid pulse pile up. Acquisition times up to 150 s achieved sufficient photon statistics for fitting. Excitation was at 890 nm. FRET efficiency (E) is related to the molecular separation of donor and acceptor and the fluorescence lifetime of the interacting fraction by:

$$E = R_0^6/(R_0^6 + R^6) = 1 - (\tau_{DA}/\tau_D)$$

where R_0 is the Förster radius, R the molecular separation, τ_{DA} is the lifetime of the interacting fraction and τ_D the lifetime of the donor in the absence of acceptor. mTFP1 demonstrated an average fluorescence lifetime in the uncomplexed state of 2.98 ns.

Expression and purification of F40 for force calibration. F40 flanked by a sequence containing a single cysteine and a thrombin cleavage site was inserted into pGEX-4T3. *Escherichia coli* BL21(DE3) pLysS competent cells were transformed and expression was induced with 0.5 mM IPTG. The cell pellet was lysed using 2 mg ml^{-1} lysozyme and affinity purification of GST–F40 was performed using GSTrap 4B prepacked columns (GE Healthcare). GST–F40 was eluted in 10 mM glutathione and thrombin was added to a final concentration of 10 mg ml^{-1} for 6 h at 4 °C. The thrombin/GST–F40 mixture was then separated on a Superdex75 column and purified with reverse-phase chromatography. The F40 elution peak was analysed and confirmed by mass spectrometry and speed vacuumed to dryness.

Preparation of the TSModCy for fluorescence force spectroscopy. Two handle DNAs with 5′-amine modifications (5′-CCCACGCGCGACTACCCAGC-3′ and 5′-GCCTCGCTGCCGTCGCCA-3′) were reacted with 200× molar excess of succinimidyl 4-[N-maleimidomethyl]cyclohexane-1-carboxylate (SMCC). Un-reacted SMCC was removed by fast protein liquid chromatography (FPLC) purification and modified DNA handles were incubated with dried F40 peptide (1:1) in 50 mM Tris buffer (pH 7.5) overnight at 4 °C. Annealing with Cy3- and Cy5-labelled strands was performed by incubation of 250 pmol of the DNA-modified F40 peptide, 250 pmol of biotinylated strand (5′-biotin-TGGCGACGGCAGCGAGGC-Cy5-3′) and 250-pmol of single-stranded (ss) DNA containing a λ-DNA cos site (5′-GGGCGGCGACCTGCTGGGTAGTCGC GCGTGGG-Cy3-3′) in 10 mM Tris-HCl (pH 8.0) and 50 mM NaCl overnight at room temperature. For fluorescence force experiments, λ-DNA (Promega) was attached to the pre-annealed product as described previously[2]. Subsequently, the digoxigenin-labelled oligonucleotide complementary to the cohesive end-site of λ-DNA was added (5′-AGGTCGCCGCCCTTT-digoxigenin-3′). Thus, the complete construct for the force sensor calibration contained a single digoxigenin tag on λ-DNA and a biotin tag at the DNA-F40 construct.